



Effects of future sea-level rise on tidal processes on the Patagonian Shelf



Stacey J. Carless^a, J.A. Mattias Green^{a,*}, Holly E. Pelling^{a,b}, Sophie-Berenice Wilmes^a

^aSchool of Ocean Sciences, Bangor University, Menai Bridge, Anglesey LL59 5AB, UK

^bNational Oceanography Center, Liverpool L3 5DA, UK

ARTICLE INFO

Article history:

Received 3 February 2016

Received in revised form 8 July 2016

Accepted 11 July 2016

Available online 14 July 2016

Keywords:

Tides

Sea-level rise

Tidal mixing

Numerical tidal model

Patagonian Shelf

ABSTRACT

The response of tidally driven processes on the Patagonian Shelf to sea-level rise (SLR) is revisited using large but realistic levels of change in a numerical tidal model. The results relate to previous studies through significant differences in the impact, depending on how SLR is implemented. This is true for how the boundary at the coastline is treated, i.e., if we allow for inundation of land or assume flood defences along the coast, but also for how the sea-level change itself is implemented. Simulations with uniform SLR provide a different, and slightly larger, response than do runs where SLR is based on observed trends. In all cases, the effect on the tidal amplitudes is patchy, with alternating increases and decreases in amplitude along the shelf. Furthermore, simulations with a realistic future change in vertical stratification, thus affecting tidal conversion rates, imply that there may be a small but significant decrease in the amplitudes along the coast. Associated processes, e.g., the location of mixing fronts and potential impacts on biogeochemical cycles on the shelf are also discussed.

© 2016 The Authors. Published by Elsevier B.V. This is an open access article under the CC BY license (<http://creativecommons.org/licenses/by/4.0/>).

1. Introduction

Global sea-level rise (SLR) occurred at an average rate of 1.7 mm yr^{-1} during the 20th century, and has since accelerated to 3.2 mm yr^{-1} (Church et al., 2013; Church and White, 2011a, 2006b; Woodworth et al., 2011). The global change in sea-level at the end of the 21st century will therefore most likely be between 0.63–0.98 m (Church et al., 2013). However, due to uncertainties in the contribution of ice melt it is possible that this rate is severely underestimated (Nicholls et al., 2011), and by the year 2500 the SLR signal from Antarctica alone may exceed 5 m under the RCP4.5 scenario, and over 12 m under RCP8.5 (DeConto and Pollard, 2016). Several papers have recently investigated how large levels of future SLR may impact on the tides on the European Shelf (Pelling and Green, 2014b; Pickering et al., 2012; Ward and Pelling, 2012) and in the Gulf of Maine (Pelling and Green, 2013a). Furthermore, Pelling et al. (2013b) showed that anthropogenic land reclamation in the Bohai Sea has led to changes in the tide equivalent to those which could be expected from realistic levels of future SLR, and Clara et al. (2015) investigated the response of the Patagonian Shelf tides to uniform sea-level rise, and find significant changes in tidal dissipation rates and the location of tidal mixing fronts. They also suggest that the M_2 amplitude changes non-uniformly with (uniform) SLR.

Here, we revisit the Patagonian Shelf and investigate the sensitivity of the tides and tidally driven processes there to various levels of homogenous and spatially varying SLR.

The Patagonian Shelf (Fig. 1) is a tidally dynamic region (see, e.g., Glorioso and Flather, 1997; Moreira et al., 2011), with a very different geometry to other investigated areas: the Patagonian Shelf is zonally narrow and stretched meridionally. It is also generally quite shallow in the north, with a depth of less than 10 m in Rio de la Plata, whereas the southern part of the domain is deeper. For example, the main portion of Golfo San Matias is deeper than 100 m, with a sill at 60 m, and that Bahia Blanca is mostly shallower than 50 m. This leads to different tidal dynamics compared to the complex topography of the European Shelf (Ward and Pelling, 2012), and the embayment-like Gulf of Maine (Pelling and Green, 2013a) and Bohai Sea (Pelling et al., 2013b). Furthermore, Arbic et al. (2009) and Arbic and Garrett (2009) suggest that the Patagonian Shelf may be near-resonant, which would make it highly sensitive to future SLR (see also Webb, 1976).

As discussed by Clara et al. (2015), changes in the tides on the Patagonian Shelf could impact the local biogeochemistry. The Patagonian Shelf is one of the world's largest sinks of CO_2 , with an annual mean air-sea CO_2 flux of $-3.7 \times 10^{-3} \text{ mol m}^{-2} \text{ day}^{-1}$ (Bianchi et al., 2009b). However, there is a strong spatial variability associated with the locations of tidal mixing fronts. Well mixed coastal waters in Bahia Grande and Golfo San Matias are sources of CO_2 with fluxes to the atmosphere of over 40 mmol day^{-1} , whereas the stratified midshelf is a strong sink with drawdown rates reaching

* Corresponding author.

E-mail address: m.green@bangor.ac.uk (J. Green).

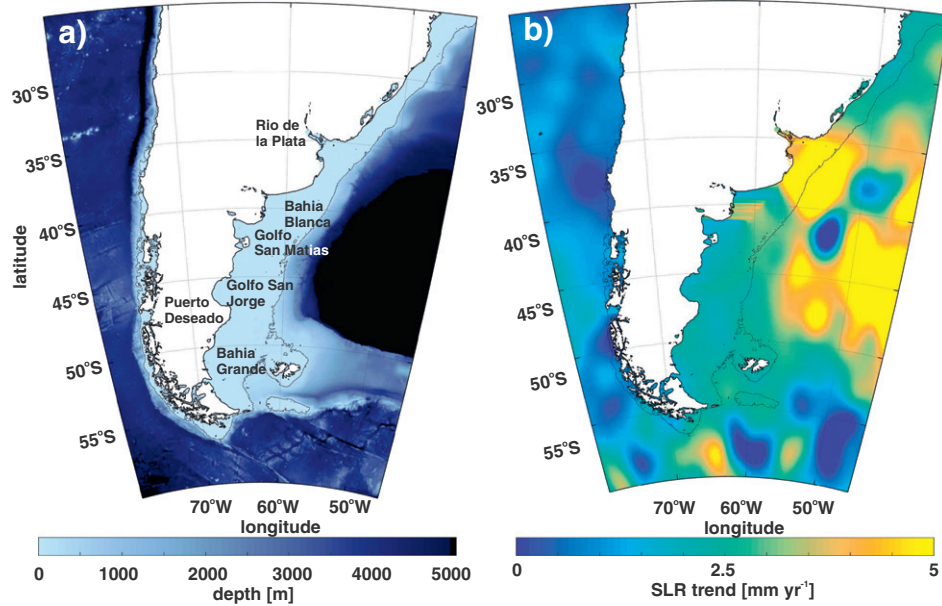


Fig. 1. a) The bathymetry of the domain from the ETOPO database (Amante and Eakins, 2009). Note that for numerical reasons the simulations were made for the domain shown here, but for clarity we are zooming in on the Patagonian Shelf when displaying results. Furthermore, there is no impact of SLR on tides in the Pacific or the northern part of the domain. b) Observed SL trends using satellite altimetry in mm yr⁻¹ from Henry et al. (2014).

–55 mmol day⁻¹ (Bianchi et al., 2005a). High phytoplankton concentrations are also associated with the frontal system (e.g. Acha et al., 2004), and the fronts have been described as the “axes for the distribution” of the Argentine anchovy (*Engraulis anchoita*; Hansen et al., 2010). They are also spawning sites for a number of other commercial species, e.g., hake and squid (Acha et al., 2004; Alemany et al., 2014), and they influence the concentration of Patagonian scallop (Orensanz et al., 1991). Consequently, any shift in the location of the tidal mixing fronts may have profound biological and ecological impacts.

The location of tidal mixing fronts can be determined by the Simpson–Hunter index, χ (Simpson and Hunter, 1974):

$$\chi = \frac{h}{|u|^3} \quad (1)$$

where h is water depth and $|u|$ the magnitude of the tidal current. In temperate waters a tidal mixing front is typically found on contours of $\log_{10}(\chi) \sim 2.5$ (Simpson and Bowers, 1981; Simpson and Hunter, 1974), and it is evident from Eq. (1) that even a small change in tidal velocity, e.g., due to SLR or future warming, can have a large impact on the location of the fronts. We can therefore expect future SLR to have far-reaching impacts on the Patagonian Shelf, not just on the physical system in the area, but also on local biochemistry and ecology.

Virtually all previous investigations of tides and SLR, both global and regional, have used a uniform SLR over the domain (e.g., Clara et al., 2015, Green, 2010, Pelling and Green, 2013a, Pelling et al., 2013a, Pickering et al., 2012). However, the observed SL trends shown in Fig. 1b indicate that the SL change over the Patagonian Shelf is far from uniform, with an average trend over the domain of +2.7 mm SLR yr⁻¹ (see Henry et al., 2014, data available from <http://sealevel.colorado.edu/content/map-sea-level-trends>). Here, we will therefore reinvestigate how the tides on the Patagonian Shelf may respond to various levels of non-uniform SLR based on the data in Fig. 1b, and compare the results using the trend data to equivalent levels of uniform SLR. Several processes can contribute to

variations in local SLR, such as uplift/subsidence land movement, climatic changes in wind patterns and changes in offshore ocean currents like a potential weakening of the Gulf Stream (e.g., Ezer, 2013). In this study, however, focus is not on why SLR is spatially variable, but on how SLR affects (shelf sea) tides. Also, the only actual observation of spatially varying SLR is the trend data in Fig. 1b, we would like to refrain from speculating on causes of the SLR in the present paper. However, because shelf sea tides can be sensitive to changes in tidal conversion around the shelf break we will also investigate how the Patagonian shelf tides may be influenced by some aspects of future warming. We say some aspects, because this is an investigation into potential changes of tidal processes on the Patagonian Shelf. Consequently, we are not discussing large scale ocean circulation or how it may change in the future.

The overarching question here, how the tides on the Patagonian Shelf respond to various levels of (non-uniform) SLR, will be answered using an established numerical tidal model used for similar work in a number of publications (e.g., Green, 2010, Green and Huber, 2013, Pelling and Green, 2013a, Pelling et al., 2013b, Wilmes and Green, 2014). The difference between previous investigations of tides and SLR is 4-fold: we will use a SLR signal based on observed trends, we will investigate changes in the tides due to future warming, we use an unprecedented model resolution of the Patagonian shelf at 1/30° in both latitude and longitude leading to a very high accuracy, and we will put the changes into a dynamical context. The model, simulations, and computations are described in the next section, whereas the results are presented in Section 3. The paper concludes in Section 4 by a discussion, the conclusions, and a future outlook.

2. Modelling tides

2.1. OTIS

The simulations were done using the Oregon State University Tidal Inversion Software (OTIS; see Egbert et al., 2004, Green and Nycander, 2013). The domain is shown in Fig. 1 and runs were done

using a horizontal resolution of $1/30^\circ$ in both latitude and longitude. OTIS provides a numerical solution to the shallow water equations, but the non-linear advection terms and the horizontal diffusion are generally neglected without loss of accuracy (Egbert et al., 2004). The forcing consists of the astronomic tide-generating force applied over the domain, and prescribed tidal elevations and -phases applied at the open boundary (see below for sources). Energy is dissipated through a quadratic bed-friction term and a linear tidal conversion scheme representing the energy losses to internal tides. We thus solve

$$\frac{\partial \mathbf{U}}{\partial t} + \mathbf{f} \times \mathbf{U} = -gh\nabla(\eta - \eta_{SAL}) + \mathbf{F}_b + \mathbf{F}_w + \boldsymbol{\Theta} \quad (2)$$

$$\frac{\partial \eta}{\partial t} = -\nabla \cdot \mathbf{U} \quad (3)$$

where $\mathbf{U} = \mathbf{u}h$ is the depth-integrated volume transport given by the velocity \mathbf{u} times the water depth h , \mathbf{f} is the Coriolis vector, η and η_{SAL} the tidal elevation and the self-attraction and loading elevation respectively, \mathbf{F} is the dissipative stress from bed friction (subscript b) and tidal conversion (subscript w), respectively, and $\boldsymbol{\Theta}$ is the astronomic tide-generating force. We use a barotropic model with a baroclinic conversion parameterisation as it has been widely used for similar tide-only investigations (Egbert et al., 2004; Green and Huber, 2013; Green and Nycander, 2013; Pelling and Green, 2013a; Rosier et al., 2013; Wilmes and Green, 2014). It has also been benchmarked against other forward tidal models, both shallow water and full 3D models, by Stammer et al. (2014). They show that the parameterisation of baroclinic processes leads to no losses in accuracy in the surface tide in comparison to models that fully resolve the baroclinic tides.

Bed-friction is parameterised using a standard quadratic law: $\mathbf{F}_b = C_d \mathbf{U} |\mathbf{u}| / h$ ($C_d = 3 \times 10^{-3}$ is a drag coefficient, and \mathbf{u} is the total velocity vector for all the tidal constituents). The tidal conversion term, \mathbf{F}_w , is a vector given by

$$\mathbf{F}_w = C(|\nabla \cdot \mathbf{h}|)^2 \frac{N_h \bar{N}}{8\pi^2 \omega} \mathbf{U} \quad (4)$$

where $C = 50$ is a scaling factor, $\nabla \cdot \mathbf{h}$ the horizontal gradient of the topography, N the buoyancy frequency, N_h is the value of N at the sea bed, \bar{N} the average of N over depth of the entire water column, and ω the tidal frequency (Green and Nycander, 2013; Zaron and Egbert, 2006). It assumes a horizontally uniform abyssal stratification based on global averages described by $N(z) = N_0 \exp(-z/1300)$ with $N_0 = 5.24 \times 10^{-3}$. It should be noted that the tidal conversion on the Patagonian Shelf is relatively weak and almost an order of magnitude smaller than that due to friction (see below), justifying our choice of conversion scheme.

A set of sensitivity simulations were used to evaluate the performance of the model (see below for results). First, we test the dependence of the model accuracy on horizontal resolution by running simulations at $1/5^\circ$, $1/10^\circ$, $1/15^\circ$, $1/30^\circ$, and $1/60^\circ$. We use the $1/30^\circ$ as our control simulation. The reasons for not using $1/60^\circ$ are threefold. First, the TPXO8 data comes at $1/30^\circ$ resolution, making comparisons with a $1/60^\circ$ dubious since to “true” tidal amplitudes may not be resolved in smaller embayments. Also, topographic databases are generally poorly constrained at high resolution, especially away from the coastline, and, lastly, running the model at $1/60^\circ$ takes almost 10 times longer than at $1/30^\circ$. We also did a series of control sensitivity simulations at $1/30^\circ$ resolution in which the bed friction coefficient (C_d) and the tidal conversion coefficient (C) were varied independently and in combination to tune the model against the (M_2) amplitudes from the TPXO8 database. In these the drag coefficient was increased/decreased by a factor 3,

and/or the tidal conversion coefficient was changed by a factor 2 (see below for results).

The bathymetric and topographic data used was the ETOPO1 database (Amante and Eakins, 2009). Boundary forcing was provided by the TPXO8 database (<http://volkov.oce.orst.edu/tides/>) and not changed in the SLR simulations. The motivation for this is that the tides do not change much on the current boundary in coarser resolution global simulations (unpublished data by the current team). All simulations were done using forcing for the M_2 , S_2 , and K_1 constituents. The model was run for 25 days of which 15 were used for harmonic analysis to provide outputs of sea-surface amplitudes and -phases, and velocity vectors and phases for each constituent. Model validation was done using TPXO8 interpolated to the current domain using linear interpolation, and the tide gauge (TG) data presented by Moreira et al. (2011). The global PSMSL network (<http://www.psmsl.org/>) does not have TG data with long enough record to compute significant trends in the tidal amplitudes, but from Fig. 1b it is evident that SL is currently rising everywhere on the Patagonian Shelf with a rate of 2.7 mm yr^{-1} .

2.2. SLR simulations

By investigating the response to relatively large levels of sea-level rise we ensure that we obtain a significant perturbation signal in the model simulations. This will later be extrapolated back to more realistic levels of SLR. A number of studies, including the science base for the latest IPCC report (Church et al., 2013), suggest that 1 m SLR will be encountered by the end of the 21st century. Furthermore, it has recently been suggested that much stronger accelerations in SLR could occur due to enhanced Antarctic Ice Sheet melt rates (Aitken et al., 2016; DeConto and Pollard, 2016), leading to a SLR of over 5 m over the next couple of centuries.

Based on these estimates, simulations were carried out in which 1 m or 3 m SLR was uniformly implemented over the domain. These are similar to simulations done in other investigations of both the Patagonian Shelf (Clara et al., 2015) and the European Shelf (e.g., Ward and Pelling, 2012). A set of novel simulations based on the observed trend data, shown in Fig. 1b, were also done. In these the data was extrapolated to a 1 m and 3 m average SLR over the domain, to be comparable to the uniform SLR simulations. Also, the use of both implementations ensures that we can compare to other investigations. Furthermore, the sea-level changes in the trend simulations are more pronounced offshore than on the shelf, which may provide a different response of the tides. All SLR simulations, both uniform and trends, were done twice: one permitted inundation of land (“flooding” or “FL” in the following) whereas the other had vertical wall along the present coastline (henceforth “no flooding” or “NFL”) – see Pelling et al. (2013a) for a discussion.

The final simulation to be discussed implemented the effects of future warming over the area. The tidal conversion rates are strongly dependent on the strength of the vertical stratification (see Eq. (4)). Based on the results of the RCP4.5 scenario in Green and Schmittner (2014) the depth-averaged buoyancy frequency, (\bar{N} in Eq. (4)), will

Table 1

M_2 sensitivity to horizontal resolution and energy parameterisations. The simulation marked in bold is the control run in the following.

Resolution ($^\circ$)	C_d	C	RMS error (cm)	Average amplitude (cm)
1/5	0.003	50	18	42
1/10	0.003	50	14	41
1/15	0.003	50	11	40
1/30	0.003	50	<10	40
1/60	0.003	50	9	40
1/30	0.001	50	21	43
1/30	0.009	50	15	35
1/30	0.003	25	12	40
1/30	0.003	100	10	37

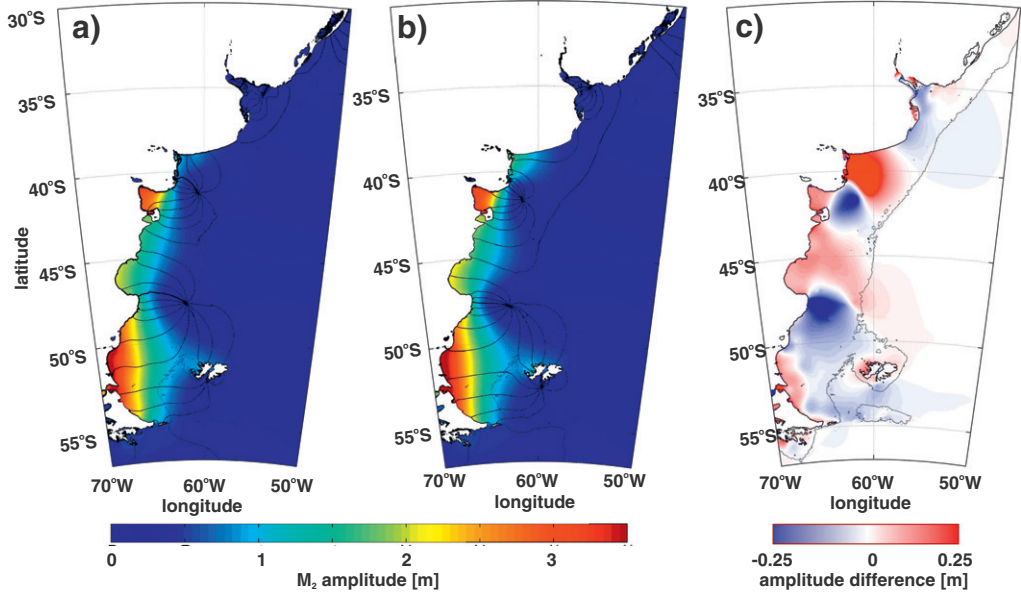


Fig. 2. a) The M_2 amplitude (colour) and relative phases (shown with 60° separation) from the TPXO8 inverse solution. b) As in a) but for the control simulation. c) The difference between panels b) and a).

increase by about 20% over the Patagonian Shelf over the next century, mainly because the surface layer will heat up more than the deeper waters. This was implemented in the tidal model in a simulations consequently called “RCP” in the following. It must be noted that we did simulations with simultaneous warming and SLR. These will not be discussed further, however, because our simulations show that the effect of SLR and warming can simply be added to give the total effect (not shown).

2.3. Computations

Tidal dissipation rates were estimated for each constituent using the theory in Egbert and Ray (2001). By taking $\mathbf{u} \cdot \nabla (\eta_{eq} + \eta_{SAL})$ (Eq. (2)) + ηg (Eq. (3)) and introducing the steady-state energy density $\rho_0 0.5 [\mathbf{h} \mathbf{u}^2 + g \eta^2]$, the well-known expression for tidal dissipation D (in W m^{-2}) can be derived after taking a time-average:

$$D = W - \nabla \cdot \mathbf{P} \quad (5)$$

The work rate, W , and the divergence of the energy flux, \mathbf{P} , are defined as

$$W = g \rho_0 \langle \mathbf{U} \cdot \nabla (\eta_{eq} + \eta_{SAL}) \rangle \quad (6)$$

$$\mathbf{P} = g \rho_0 \langle \mathbf{U} \eta \rangle \quad (7)$$

in which $\langle \rangle$ denote the time-averages. Using tidal amplitudes and currents from either the TPXO data base (for validation) or from the model simulations it is therefore possible to calculate the dissipation rate for each constituent.

3. Results

3.1. Control evaluation

The resulting root-mean-square (RMS) errors between the modelled and observed (TPXO8) M_2 amplitudes for the resolution tests

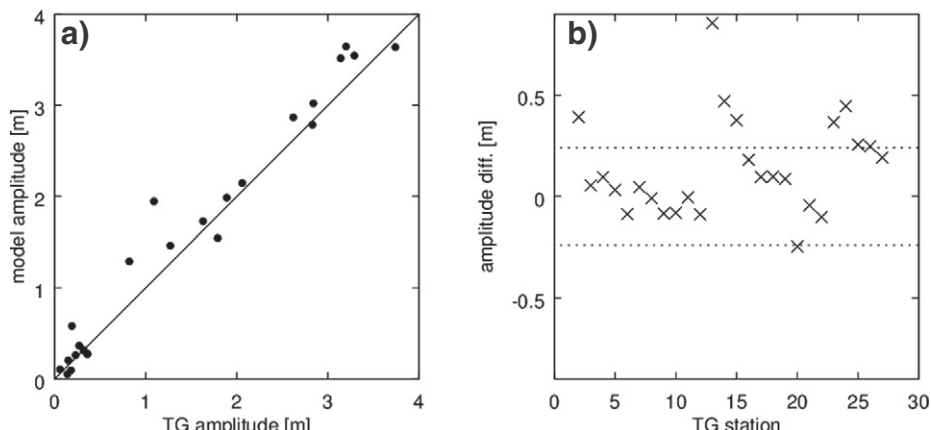


Fig. 3. a) The M_2 amplitude for the tide gauge data in Moreira et al. (2011) plotted against the modelled amplitude in the corresponding locations. The solid line is the 1 to 1 relationship. b) The difference between the tide gauge data and the modelled amplitudes for each station. The dotted lines mark ± 1 standard deviation of the difference.

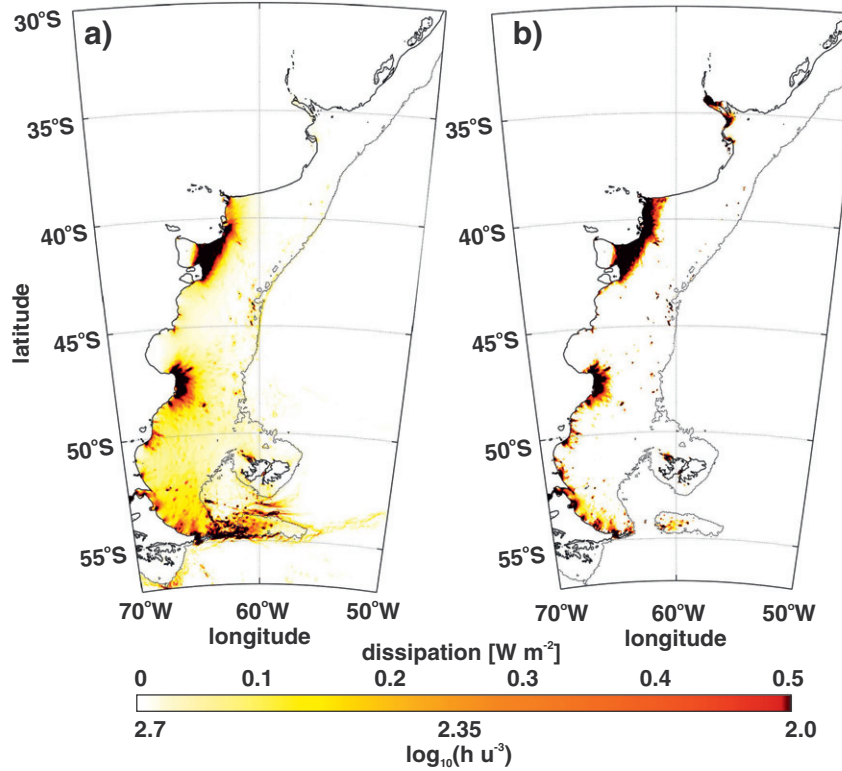


Fig. 4. a) The dissipation of energy in the M_2 band from the control simulation. b) The control $\log_{10}\chi$ computed from Eq. (1). White areas are vertically stratified, coloured patches are well mixed with the mixing increasing with increased darkness. Note the reversed colour scales.

are shown in Table 1. It is evident that higher resolution leads to a more accurate simulation, and we chose to use $1/30^\circ$ as a compromise. The results of the dissipation sensitivity runs show that the default settings mentioned above, i.e., $C_d = 0.003$ and $C = 50$, provided the most accurate result and were therefore used throughout all further simulations. Our chosen control is thus the $1/30^\circ$ simulation with default values for C_d and C .

The control simulation gave a root-mean-square (RMS) difference between the model and the TPXO8 data of just under 10 cm for M_2 , 4 cm for S_2 and 8 cm for K_1 (see Table 1 and Fig. 2). Offsets between the amplitudes between TPXO8 database and the modelled tidal amplitudes are prominent close to the two main amphidromes on the shelf. In our non-assimilated simulations the amphidrome at 42°S is displaced to the south-west and the one at 48°S is displaced

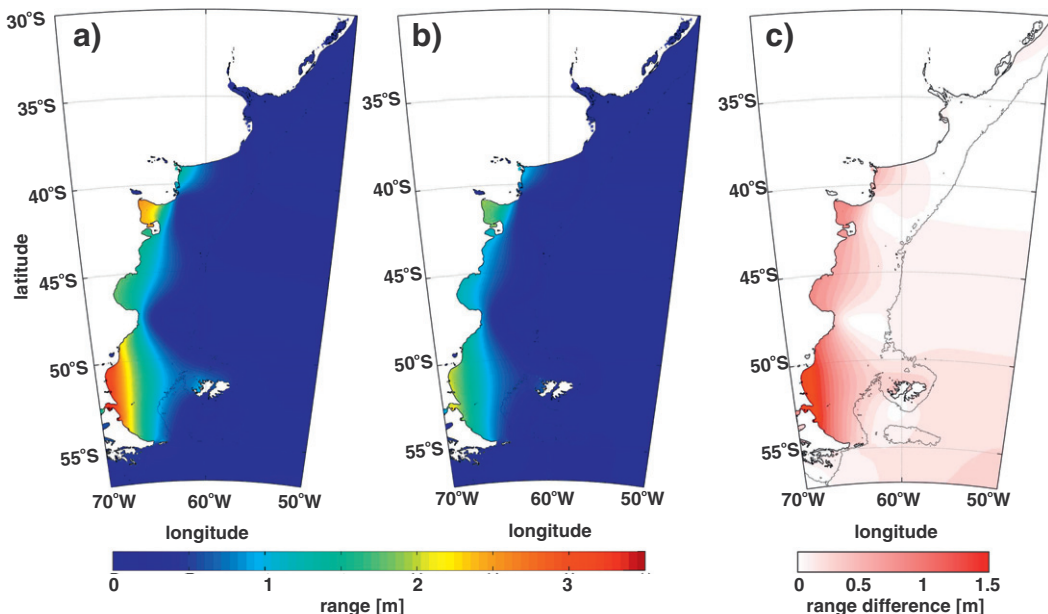


Fig. 5. a) Spring amplitudes from the control simulation. b) Neap amplitudes from the control simulation. Note the double scale bar for panels a) and b), with a) using the scale above the bar. c) Spring–neap range, e.g., the difference between panels a and b.

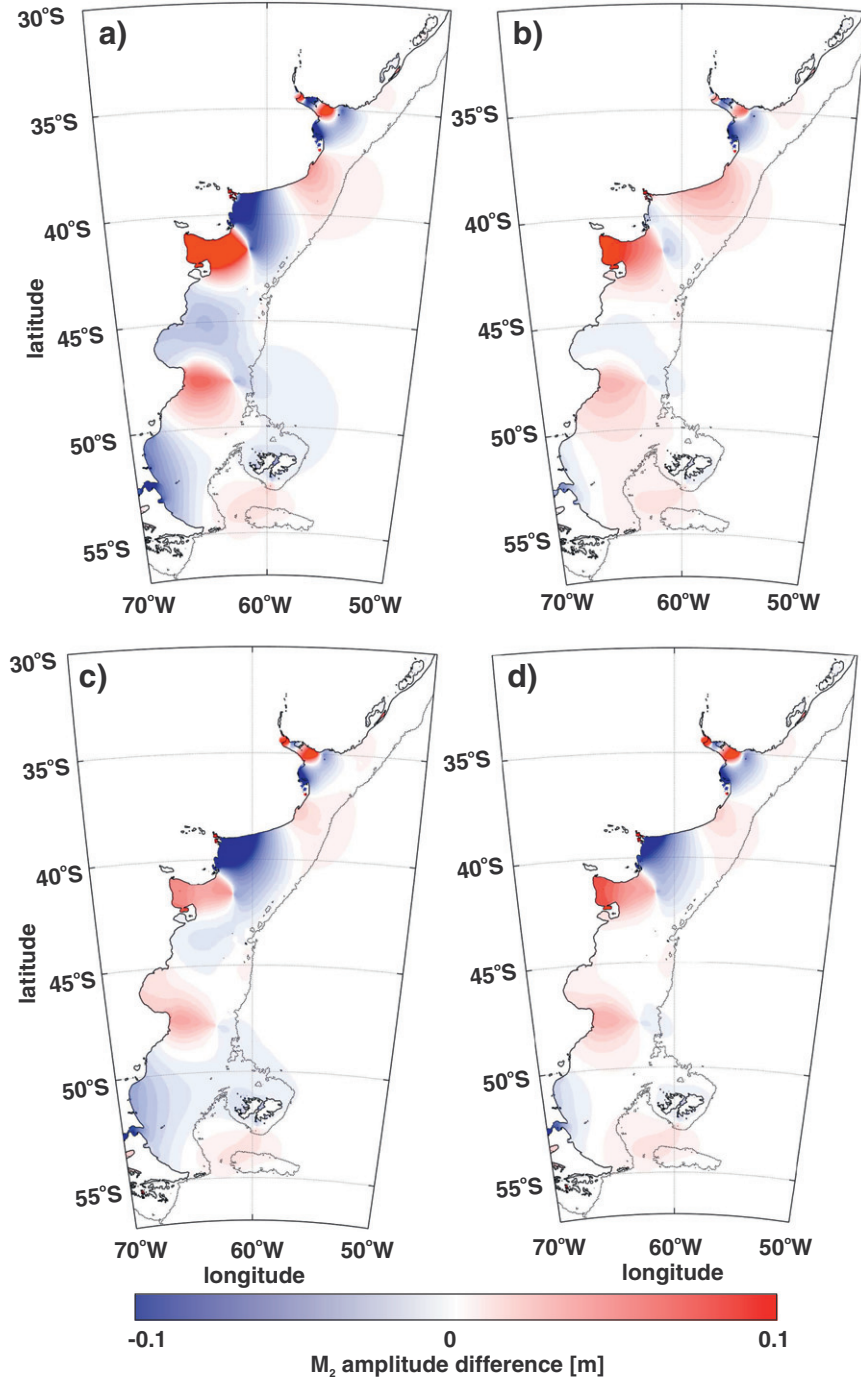


Fig. 6. a-b) The difference between SLR simulations and the control for a uniform 1 m SLR. Panel a) shows the FL and panel b) the NFL simulations, respectively. c-d) As in panels a)-b) but for the trend SLR simulation averaging 1 m SLR.

westward. This discrepancy could be due to inaccuracies in the topographic databases, which the data assimilation in TPXO8 compensates for. A comparison to the TG data in Moreira et al. (2011) gives a difference of 22 cm for M_2 (Fig. 3). There are, however, a few locations where there is a very large disagreement between the model and TG data. This is most likely due to the model not resolving these inshore areas properly, and if the 9 stations for which the difference in amplitude lies ± 1 standard deviation is omitted from the analysis the RMS difference between the model and the TG data is 11 cm for M_2 . This small error gives us confidence in the results to follow.

Although we did simulations with 3 constituents focus is on the response of M_2 in the following. This is motivated by M_2 having by far the largest signal and thus experiencing the largest changes. K_1 is excluded from the following because the results showed practically no change with SLR, whereas S_2 will be included indirectly when we discuss changes in the spring-neap cycle (chosen because of its importance in modulating primary production; Sharples et al., 2007). The control M_2 amplitudes show the common shelf-sea picture with large amplitudes on the shelf, especially in shallow embayments (Fig. 2b). The control run displays high dissipation rates in these locations in the M_2 band, as well as in southern part of the shelf (Fig. 4a).

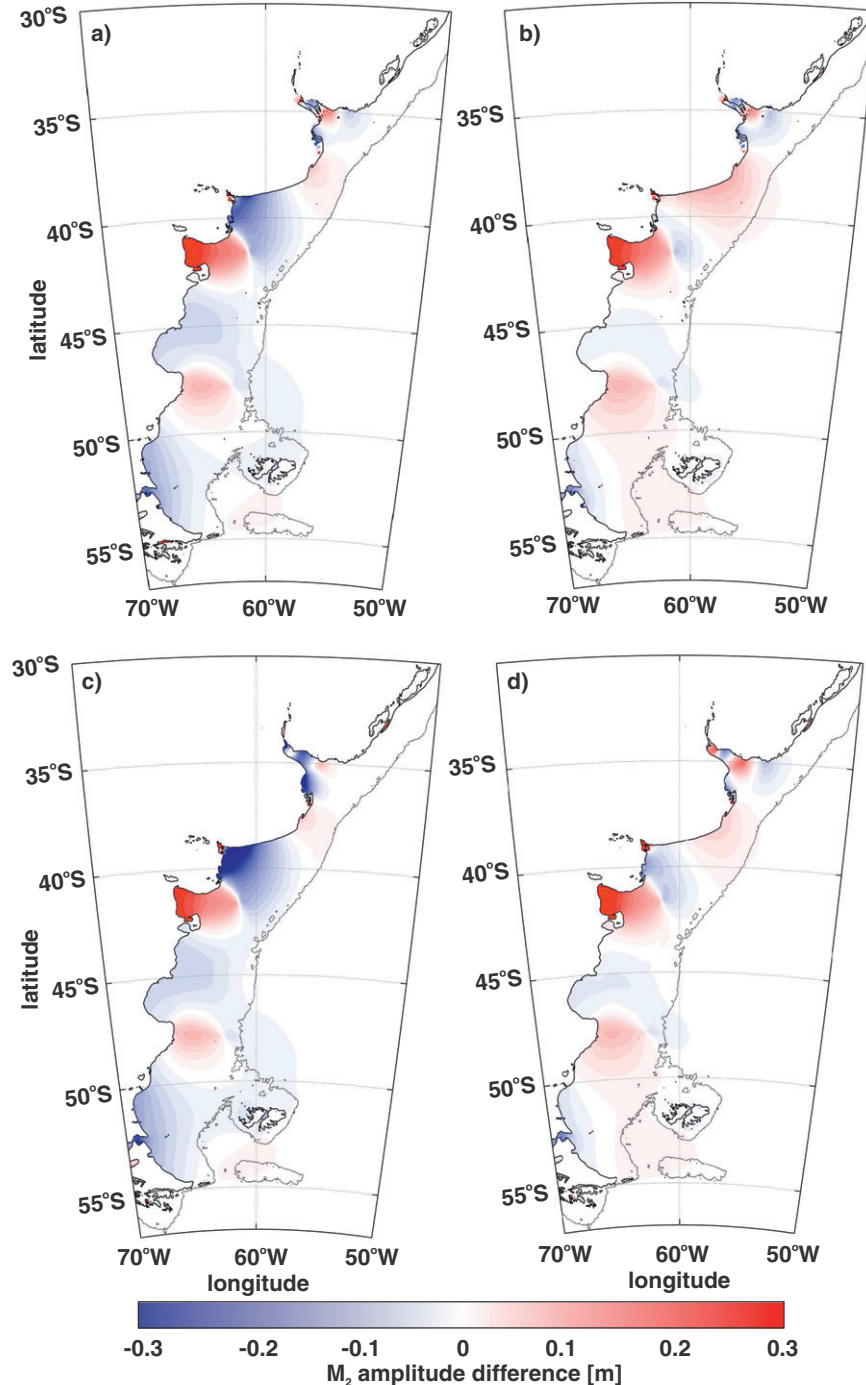


Fig. 7. As in Fig. 6 but for 3 m SLR.

This is despite relatively small tidal amplitudes in the south and due to tidal conversion there. The higher rates in shallow water are due to bed friction in areas with large velocities (not shown). These patches of high dissipation in shallow water lead to the water column being vertically well mixed there (see Fig. 4b; a $\log_{10}\chi < 2.7$ indicates mixed conditions). There is also a large spring-neap range with a 2.5 m difference between springs ($M_2 + S_2$) and neaps ($M_2 - S_2$) over large parts of the shelf (Fig. 5).

3.2. Impact on tidal amplitudes

The runs with 1 m uniform SLR and flooding show relatively large changes in tidal amplitudes (see Fig. 6a), whereas changes in the NFL

simulation are smaller (Fig. 6b). In both the FL and NFL cases there are large spatial variations, with alternating regions experiencing increases or decreases. This is indicative of shifts of the amphidromic systems on the shelf induced by the changing propagation properties of the tidal wave. This is especially true in the FL simulations, where the inundation of new land leads to areas with high dissipation rates. This in turn leads to a shift of the amphidromes towards the newly formed ocean areas, with significant system-wide impacts over the shelf (Pelling et al., 2013a; Rienecker and Teubner, 1980; Taylor, 1920).

The response of the M₂ tidal amplitudes to a uniform 3 m SLR with flooding is enhanced compared to uniform 1 m FL case, but the response is not necessarily proportional to the magnitude of SLR

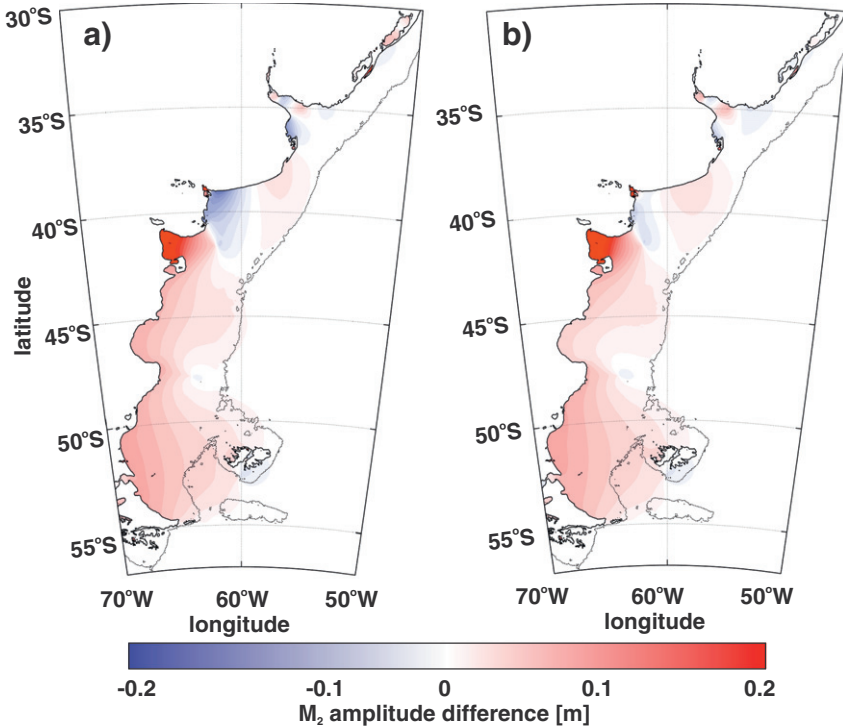


Fig. 8. Shown is the difference in spring–neap range between the 3 m trend SLR runs and the control for FL (a) and NFL (b).

(see Figs. 6b–c and 7b–c; note that the colour scales are proportional to the amount of implemented SLR in these simulations). The change in M_2 amplitude per metre SLR is larger in the 1 m SLR FL runs than in the 3 m FL simulation. The NFL runs, in contrast, appear to have a response directly proportional to the level of SLR. This is because the inundation in the FL runs has the capacity to change dissipation more than the change in water depth can in the NFL simulations. 1 m FL is more efficient in changing tidal amplitudes than 3 m FL because 1 m SLR adds an area of $0.8 \times 10^4 \text{ km}^2$ to the ocean, whereas 3 m SLR only adds another $0.2 \times 10^4 \text{ km}^2$ for a total flooded area of $1.0 \times 10^4 \text{ km}^2$. With such a vast expansion of very shallow water area we can expect large changes increases in tidal dissipation, resulting in amphidromic systems relocating – usually towards the newly formed ocean areas – with amplitude changes following (see Pelling et al., 2013a, for a discussion).

The 1 m trend simulations, both FL and NFL, show a spatial response quite similar to those with 1 m uniform SLR although the amplitude changes in the trend FL simulation are enhanced compared to the uniform case (cf. Fig. 6a–b and c–d). The 3 m trend simulation shows a similar signal to the 3 m uniform simulations (cf. Fig. 7a–b and c–d), and reproduces the 1 m trend SLR signal in spatial variation but with a slightly larger range of the changes (Figs. 6c–d and 7c–d). The trend FL run exhibits a larger change than the corresponding NFL simulation. Altogether, these results show that the Patagonian Shelf is quite sensitive to the way SLR is implemented, both in terms of the structure of the SL change and whether or not flooding is allowed.

The non-proportional response and sensitivity to implementation is an indication of the Patagonian Shelf being near-resonant. This is further supported by the changes in the spring–neap cycle (see Fig. 8 for the 3 m trend results): the spring–neap range increases throughout the southern part of the domain, except in Golfo San Jorge where it decreases. The changes are on the order of 0.2 m, or some 10–20% of the control range in Fig. 5c, but the fact that there is an overall increase in range implies that M_2 has changed more than S_2 . This

lends support to the suggestions that the Patagonian Shelf is (near) resonant for the M_2 frequency and that it is actually moving towards M_2 resonance with SLR (see Webb, 1976; Arbic and Garrett, 2009; Arbic et al., 2009, for a discussion).

3.3. Dissipation and further consequences

Because the changes in tidal amplitudes are largest in shallow water, we will focus our attention on the dissipation in waters shallower than 200 m and the 3 m SLR simulations. We chose the 3 m simulations because of the larger signal. The results are summarised in Table 2 and Fig. 9. The total dissipation decreases compared to the control in all four 3 m SLR simulations due to an overall reduced dissipation in shallow water (Table 2). The FL scenarios show a larger reduction than NFL scenarios and there is a large spatial variability in all simulations (Fig. 9). Bahia Blanca and the outer part of the Golfo San Matias experience an enhanced dissipation rate in all simulations, whereas the headland around Puerto Deseado and Bahia Grande and the southern part of the shelf consistently see a decreased dissipation rate. Where amphidromes move away from (towards) the shelf an enhanced (reduced) dissipation can be found, as in Golfo San Matias and Golfo San Jorge. Bahia Grande consistently

Table 2

Summary of the dissipation results for the control, 3 m SLR runs, and the climate change simulation (RCP4.3). “Total” denotes the horizontally integrated dissipation rate in GW over the entire domain, whereas “Shallow” is the rate in water shallower than 200 m. “% well mixed” marks the percentage of the ocean surface area which is vertically well mixed based on Eq. (1) (see Fig. 4).

Run	Total	Shallow	% well mixed
Control	153	128	2.6
Trend FL	144	119	2.3
Trend NFL	149	123	2.3
Uniform FL	140	116	2.7
Uniform NFL	148	123	2.7
RCP4.5	151	122	2.4

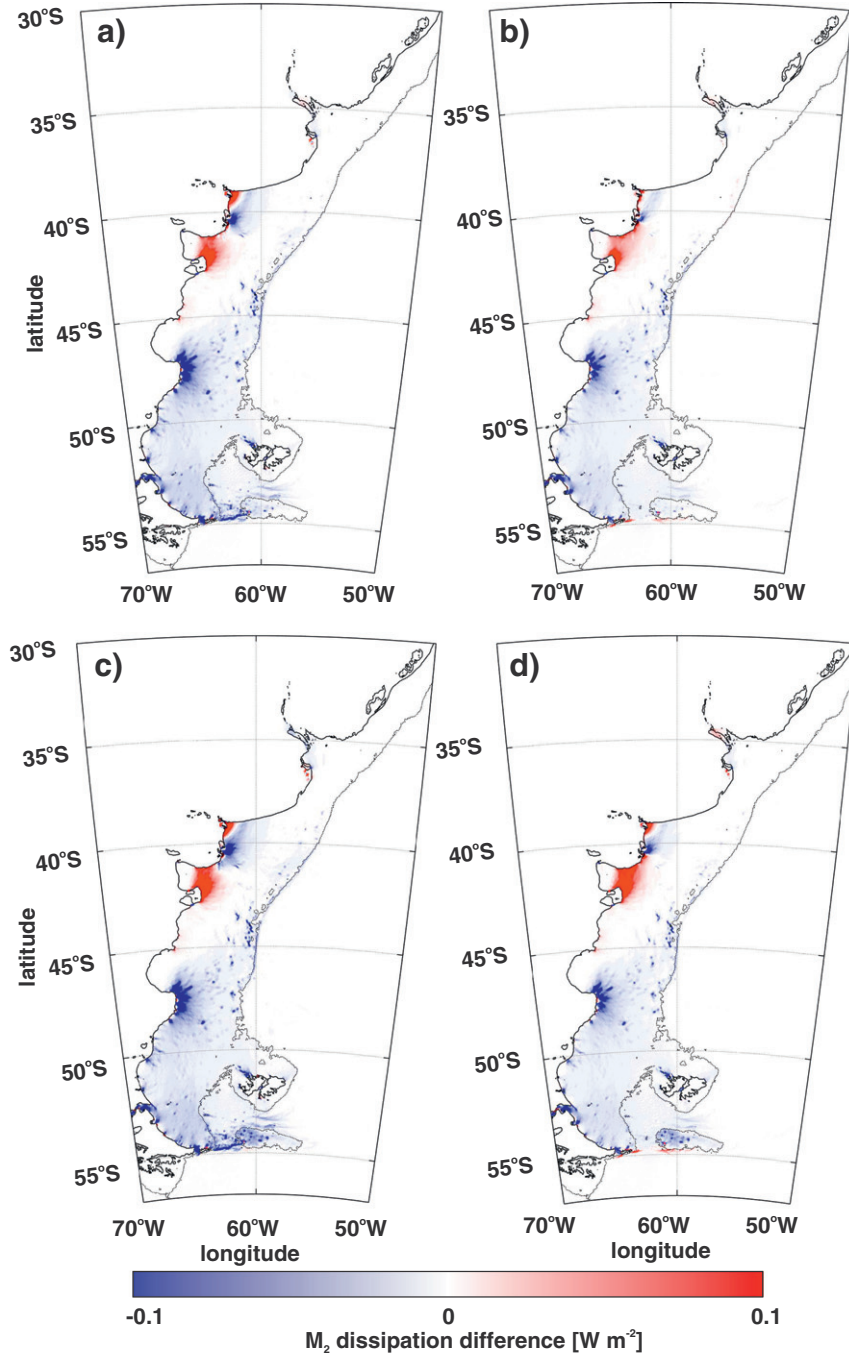


Fig. 9. The computed M_2 tidal dissipation rates for 3 m SLR for uniform FL (a), NFL (b), trend FL (c) and trend NFL (d).

experiences a reduced amplitude and associated dissipation rate and it is quite likely that the reduced dissipation around Puerto Deseado is linked to the reduced energetics of the tidal wave after passing over the wide Bahia Grande.

The changes in tidal dissipation, which imply a shelf scale decrease of the tides (although with large spatial variations), have further consequences. For example, using Eq. (1) it can be shown that the vertically mixed areas of the shelf decrease with trend SLR but increase slightly with uniform SLR (see Table 2 for a summary and Fig. 4b for the control situation). The decreases in mixed area in the trend simulations suggest that the tidal mixing fronts have shifted towards the coast in these cases, but moved ever so slightly offshore in the uniform simulations. This may have consequences for other

processes, e.g., sediment transport and primary production, since a 0.1% change in mixed area represents an area of 10,000 km². It also highlights the need for further studies of the impact of realistically implemented SLR in shelf seas.

3.4. Effects of climate change

Here we only consider the large scale changes in stratification that may influence conversion, and thus directly impact on the tides. Consequently, we disregard any other impacts on the marine system, e.g., shear production, baroclinicity and steric effects (beyond those included in the trend data). The RCP simulation, with enhanced tidal conversion, exhibits a decrease in M_2 amplitudes of a few cm across

the shelf, whereas the drop in amplitude at the coastline approaches 15 cm (Fig. 10a). The reason for this decrease is that the increases in vertical stratification enhance the tidal conversion at the shelf break. This dissipation of energy at the shelf break leads to reduces tidal amplitudes. Although the effect is small it is of similar magnitude to the 1 m SLR runs, suggesting that future simulations of realistic SLR on tides, e.g., for management purposes, should also include changes in stratification.

4. Discussion

Here we show that the tidal regime of the Patagonian shelf is sensitive to SLR and changes in stratification, both of which are potential impacts of future climate change. The M_2 tides are close to resonance and any change to this balance will result in disproportionately large impacts. The impact of flooding (due to SLR) results in a larger change in tidal energy dissipation and movement of amphidromic points than increasing the water depth alone (NFL). Thus, the impact of SLR with flooding of new land is larger than SLR with no flooding. Increased stratification results in higher levels of tidal conversion over the shelf break, thus resulting in a decrease in tidal amplitude towards the coast. Both processes have been shown to be important when simulating the impact of SLR on the tidal regime of the Patagonian Shelf.

Sea level in the study area would rise about 0.2 m by 2100 if the SLR rate remains unchanged, but many studies show that SLR is accelerating both globally (e.g. Church and White, 2006b) and locally (e.g. Ezer, 2013). The effect of small sea level change is difficult to accurately simulate, so experiments with 1 m and 3 m SLR were conducted as well. We can then do a regression using a cubic spline on our control and trend 1 m and 3 m SLR amplitudes by fitting a cubic spline (e.g., Emery and Thomson, 1996). The result from the fitting can then be used to obtain an estimate of what impact 0.2 m SLR would have on the tidal amplitudes. The resulting

amplitude changes are plotted in Fig. 11 and although they are small, they would add another 20–25% of sea-level variability on top of the 0.2 m SLR signal near the coast. Furthermore, the fact that we actually obtain a signal at all for such small levels of SLR again highlights the sensitivity of the Patagonian Shelf to changes in sea-level and, ultimately, bathymetry and coastline change. A further test of the robustness of the present results was done by doing simulations using the sea-level fingerprint signal of a total collapsing West Antarctic Ice Sheet (Gomez et al., 2010; results not shown). This would induce an average of some 3 m SLR over our domain, with a decrease in SL of around a metre in the south and up to 5 m SLR in the northern part. However, the response of the tides in our domain is virtually identical to that of the 3 m uniform simulation, and these simulations are not discussed further.

In all our simulations the non-linear terms in the shallow water equations have been neglected and a tidal conversion methodology has been used, however we would expect errors as a result of this to be small. Furthermore the modelled signals are generally larger than the model error calculated, which gives us confidence in the results presented.

Here, we have addressed the potential impacts of climate change on the tidal regime on the Patagonian Shelf. The tides represent one crucial component in the dynamic regime, and further evaluations of the impacts of changes in the large scale ocean circulation are left for future investigations. The values of tidal dissipation over the shelf (140–153 GW) are larger than those found by Egbert and Ray (2001) (95–138 GW) and in TPXO8 (131 GW). There are a number of potential reasons for this difference, including the error in our model simulations generally overestimating the tide, slightly different domains (than in Egbert and Ray, 2001), unresolved topography in the conversion scheme Eq. (4), and a more up-to-date bathymetry in our simulations. Our model runs are generally biased high (cf. Fig. 2). Because of the cubic relationship between dissipation due to friction and velocity, the overall loss is biased high

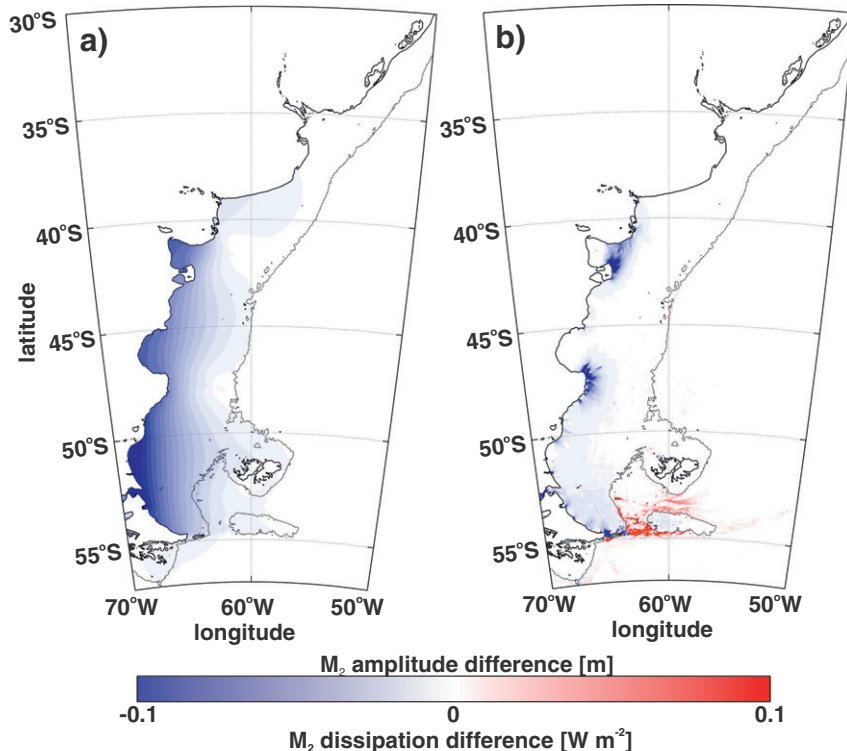


Fig. 10. The impact on the M_2 amplitude of future changes in stratification from the RCP4.5 scenario on tidal conversion. Panel (a) shows change in amplitude, and panel (b) shows change in dissipation.

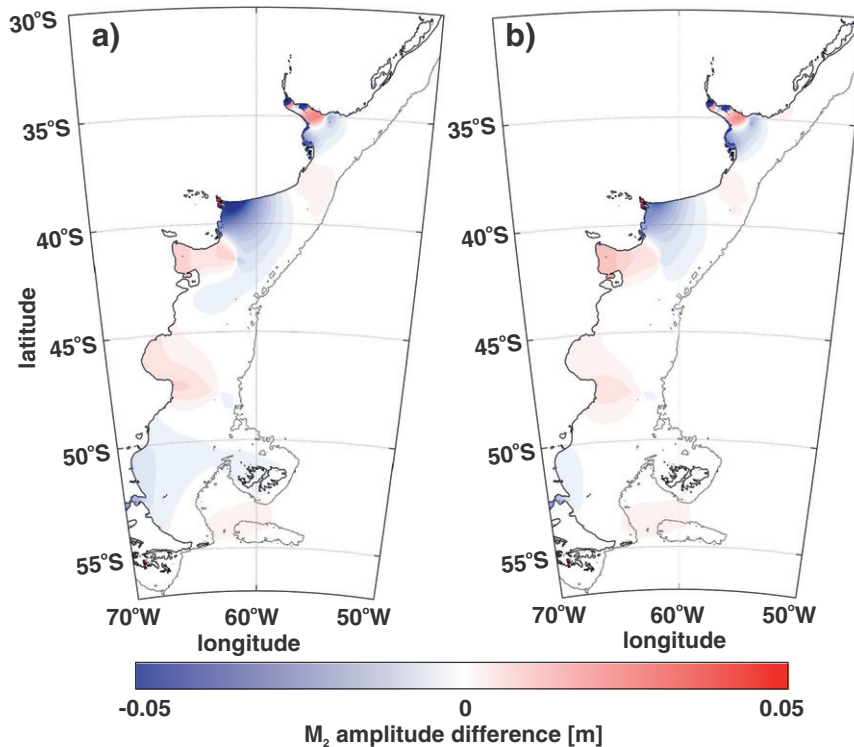


Fig. 11. Results of the interpolation to 0.2 m trend SLR for FL (a) and NFL (b). Note that for clarity the colour scale is *not* proportional to the level of SLR in this figure.

(see Egbert et al., 2004, for a similar discussion). This is supported further by the even higher rates in the low-resolution simulations, which overestimate the shelf tide even more (see also Egbert et al., 2004).

This study highlights the importance of using spatially varying sea level trends, correct implementation of SLR at the coastline and future stratification, when simulating future tidal regimes. The tidal fronts of the Patagonian shelf are associated with high biological production, which supports economically important fisheries and CO₂ drawdown. Our simulations suggest that SLR may result in changes to the vertical structure of the water column and it is possible this may have important impacts on the biology, biochemistry and ecology of the system.

Tides on the Patagonian Shelf have proven to be sensitive to future climate changes due to the close proximity of the M₂ tides to resonance. Even though the impact of SLR on the tidal amplitudes is moderate, there are differences in the results depending on how SLR is implemented, both in terms of flooding and the structure of the SLR signal. To obtain reliable estimates of future effects it is therefore necessary to use the correct stratification in the tidal conversion parameterisations and a SLR signal based on observed trends.

Acknowledgements

Funding was provided by Natural Environmental Research Council through the FASTNEt and PycnMix projects (NE/I030224/1 to JAMG and NE/L003600/1 to HEP, respectively), through a School of Ocean Sciences Deeming summer bursary (awarded to SJC), and from a Fujitsu PhD studentship (SBW). The simulations were done using HPC Wales, and the technical support from Ade Fewings and extra simulations by Emily Bamber are gratefully acknowledged. Discussions with John Simpson improved the manuscript, as did comments from two anonymous reviewers and from the Editor

(Professor Hoffmann). The model simulations are available from the corresponding author.

References

- Acha, E.M., Mianzan, H.W., Guerrero, R., Favero, M., Bava, J., 2004. Marine fronts at the continental shelves of austral south america - physical and ecological processes. *J. Mar. Syst.* 44, 83–105.
- Aitken, A.R.A., Roberts, J.L., van Ommen, T.D., Young, D.A., Golledge, N.R., Greenbaum, J.S., Blankenship, D.D., Siegert, M.J., 2016. Repeated large-scale retreat and advance of totten glacier indicated by inland bed erosion. *Nature* 533, 385–389.
- Alemany, D., Acha, E., Irribarne, O., 2014. Marine fronts are important fishing areas for demersal species at the Argentine Sea (Southwest Atlantic Ocean). *J. Sea Res.* 87, 56–67.
- Amante, C., Eakins, B.W., 2009. Etopo1 1 arc-minute global relief model: procedures, data sources and analysis. NOAA Technical Memorandum NESDIS NGDC-24. National Geophysical Data Center, NOAA 31. <http://dx.doi.org/10.7289/V5C8276M>.
- Arbic, B.K., Garrett, C., 2009. A coupled oscillator model of shelf and ocean tides. *Cont. Shelf Res.* <http://dx.doi.org/10.1016/j.csr.2009.07.008>.
- Arbic, B.K., Karsten, R.H., Garrett, C., 2009. On tidal resonance in the global ocean and the back-effect of coastal tides upon open-ocean tides. *Atmosphere-Ocean* 47, 239–266.
- Bianchi, A.A., Bianucci, L., Piola, A.R., Pino, D.R., Schloss, I., Poisson, A., Balestrini, C.F., 2005. Vertical stratification and air-sea Co₂ fluxes in the Patagonian Shelf. *J. Geophys. Res. Oceans* 110 (C7), C07003. URL <http://dx.doi.org/10.1029/2004JC002488>.
- Bianchi, A.A., Pino, D.R., Perlender, H.G.I., Osiroff, A.P., Segura, V., Lutz, V., Clara, M.L., Balestrini, C.F., Piola, A.R., 2009. Annual balance and seasonal variability of sea-air Co₂ fluxes in the Patagonia sea: their relationship with fronts and chlorophyll distribution. *J. Geophys. Res. Oceans* 114 (C3), C03018. URL <http://dx.doi.org/10.1029/2008JC004854>.
- Church, J., Monselesan, D., Gregory, J., Marzeion, B., 2013. Evaluating the ability of process based models to project sea-level change. *Environ. Res. Lett.* 8, 014051.
- Church, J., White, N., 2011. Sea-level rise from the late 19th to the early 21st century. *Surv. Geophys.*
- Church, J.A., White, N.J., 2006. A 20th century acceleration in global sea-level rise. *Geophys. Res. Lett.* 33, L01602.
- Clara, M.L., Simionato, C.G., D'Onofrio, E., Moreira, D., 2015. Future sea level rise and changes on tides in the Patagonian continental shelf. *J. Coast. Res.* 31, 519–535.
- DeConto, R.M., Pollard, D., 2016. Contribution of Antarctica to past and future sea-level rise. *Nature* 531, 591–597.

- Egbert, G.D., Bills, B.G., Ray, R.D., 2004. Numerical modeling of the global semidiurnal tide in the present day and in the last glacial maximum. *J. Geophys. Res.* 109, C03003. <http://dx.doi.org/10.1029/2003JC001973>.
- Egbert, G.D., Ray, R.D., 2001. Estimates of M2 tidal energy dissipation from *Topex/Poseidon* altimeter data. *J. Geophys. Res.* 106, 22475–22502.
- Emery, W.J., Thomson, R.E., 1996. Data Analysis Methods in Physical Oceanography. 2nd edition, Pergamon Press. 650pp
- Ezer, T., 2013. Sea level rise, spatially uneven and temporally unsteady: why the U.S. East Coast, the global tide gauge record and the global altimeter data show different trends. *Geophys. Res. Lett.* 40, 5439–5444.
- Glorioso, P., Flather, R., 1997. The Patagonian Shelf tide. *Prog. Oceanogr.* 40, 263–283.
- Gomez, N., Mitrovica, J.X., Tamisiea, M.E., Clark, P.U., 2010. A new projection of sea level change in response to collapse of marine sectors of the antarctic ice sheet. *Geophys. J. Int.* 180, 623–634.
- Green, J.A.M., 2010. Ocean tides and resonance. *Ocean Dyn.* 60,
- Green, J.A.M., Huber, M., 2013. Tidal dissipation in the early Eocene and implications for ocean mixing. *Geophys. Res. Lett.* 40, <http://dx.doi.org/10.1002/grl.50510>.
- Green, J.A.M., Nylander, J., 2013. A comparison of internal wave drag parameterizations for tidal models. *J. Phys. Oceanogr.* 43, 104–119.
- Green, J.A.M., Schmittner, A., 2015. Climatic consequences of a pine island glacier collapse. *J. Climate* 28, 9221–9234.
- Hansen, J., Martos, P., Madirolas, A., 2010. Relationship between spatial distribution of the Patagonian stock of Argentine anchovy, *Engraulis anchoita*, and sea temperatures during late spring to early summer. *Fish. Oceanogr.* 10 (2), 193–206.
- Henry, O., Ablain, M., Meyssignac, B., Cazenave, A., Masters, D., Nerem, R., Garric, G., 2014. Effect of the processing methodology on satellite altimetry-based global mean sea level rise over the Jason-1 operating period. *J. Geod.* 88, 351–361.
- Moreira, D., Simionato, C.G., Dragani, W., 2011. Modeling ocean tides and their energetics in the North Patagonia Gulfs of Argentina. *J. Coast. Res.* 27, 87–102.
- Nicholls, R.J., Marinova, N., Lowe, J.A., Brown, S., Vellinga, P., de Gusmao, D., Hinkel, J., Tol, R.S.J., 2011. Sea-level rise and its possible impacts given a ‘beyond 4° c world’ in the twenty-first century. *Philos. Trans. R. Soc. Lond.* 369, 161–181.
- Orensanz, J., Parma, A., Iribarne, O., 1991. Population dynamics and management of natural stocks. *Dev. Aquac. Fish. Sci.* 21, 625–713.
- Pelling, H.E., Green, J.A.M., 2013. Sea-level rise, tidal power, and tides in the Bay of Fundy. *J. Geophys. Res.* 118, 1–11.
- Pelling, H.E., Green, J.A.M., 2014. The impact of sea level rise and flood defences on tides on the European shelf. *Cont. Shelf Res.* 85, 96–105.
- Pelling, H.E., Green, J.A.M., Ward, S.L., 2013. Sea level rise on shelf sea tides: to flood or not to flood. *Ocean Dyn.* (63), 21–29.
- Pelling, H.E., Uehara, K., Green, J.A.M., 2013. The impact of rapid coastline changes on the tides in the Bohai sea, China. *J. Geophys. Res.* 118, 3462–3472.
- Pickering, M., Wells, N.S., Horsburgh, K., Green, J.A.M., 2012. The impact on the European Shelf tides by future sea-level rise. *Cont. Shelf Res.* <http://dx.doi.org/10.1016/j.csr.2011.11.011>.
- Rienecker, M., Teubner, M., 1980. A note on frictional effects in Taylor’s problems. *J. Mar. Res.* 38, 183–191.
- Rosier, S.H.R., Green, J.A.M., Scourse, J.D., Winkelmann, R., 2013. A quantification of the impact of ice-shelves on tides. *J. Geophys. Res.* 119, <http://dx.doi.org/10.1002/2013JC009240>.
- Sharples, J., Tweddle, J.F., Green, J.A.M., Palmer, M.R., Kim, Y.N., Hickman, A.E., Holligan, P.M., Moore, C.M., Rippeth, T.P., Simpson, J.H., Krivtsov, V., 2007. Spring–neap modulation of internal tide mixing and vertical nutrient fluxes at a shelf edge in summer. *Limnol. Oceanogr.* 52, 1735–1757.
- Simpson, J.H., Bowers, D., 1981. Models of stratification and frontal movements in shelf seas. *Deep-Sea Res.* 28, 727–738.
- Simpson, J.H., Hunter, J., 1974. Fronts in the Irish Sea. *Nature* 250, 404–406. <http://dx.doi.org/10.1038/250404a0>.
- Stammer, D., Ray, R.D., Andersen, O.B., Arbic, B.K., Bosch, W., Carrére, L., Cheng, Y., Chinn, D., Dushaw, B., Egbert, G., Erofeeva, S., Fok, H., Green, J., Griffiths, S., King, M., Lapin, V., Lemoine, F., Luthcke, S., Lyard, F., Morison, J., Müller, M., Padman, L., Richman, J., Shriver, J., Shum, C., Taguchi, E., Yi, Y., 2014. Accuracy assessment of global ocean tide models. *Rev. Geophys.* 52, <http://dx.doi.org/10.1002/2014RG000450>.
- Taylor, G.I., 1920. Tidal oscillations in gulfs and rectangular basins. *Proc. Lond. Math. Soc.* 20, 148–181.
- Ward, S.L., Green, J.A.M., Pelling, H.E., 2012. Tidal dynamics and sediment transport on the European Shelf with future climate change. *Ocean Dyn.* 62, 1153–1167.
- Webb, D., 1976. Model of continental-shelf resonances. *Deep-Sea Res.* 23, 1–15.
- Wilmes, S.B., Green, J.A.M., 2014. The evolution of tides and tidally driven mixing over 21,000 years. *J. Geophys. Res.* 119, <http://dx.doi.org/10.1002/2013JC009605>.
- Woodworth, P., Gehrels, W., Nerem, R., 2011. Nineteenth and twentieth century changes in sea level. *Oceanography* 24, 80–93.
- Zaron, E.D., Egbert, G.D., 2006. Estimating open-ocean barotropic tidal dissipation: the Hawaiian Ridge. *J. Phys. Oceanogr.* 36, 1019–1035.